Casimir-Lifshitz Optical Resonators: A New Platform for Exploring Physics at the Nanoscale

Victoria Esteso, Diego Frustaglia, Sol Carretero-Palacios, and Hernán Míguez**

The Casimir-Lifshitz force, F_{C-L}, has become a subject of great interest to both theoretical and applied physics communities due to its fundamental properties and potential technological implications in emerging nano-scale devices. Recent cutting-edge experiments have demonstrated the potential of quantum trapping at the nano-scale assisted by F_{C-L} in metallic planar plates immersed in fluids through appropriate stratification of the inner dielectric media, opening up new avenues for exploring physics at the nano-scale. This review article provides an overview of the latest results in Casimir-Lifshitz based-optical resonator schemes and their potential applications in fields such as microfluidic devices, bio-nano and micro electromechanical systems (NEMS and MEMS), strong coupling, polaritonic chemistry, photo-chemistry, sensing, and metrology. The use of these optical resonators provides a versatile platform for fundamental studies and technological applications at the nano-scale, with the potential to revolutionize various fields and create new opportunities for research.

1. Introduction

1.1. Casimir-Lifshitz Force

Quantum vacuum electromagnetic (EM) fluctuations confined between two bodies at nano- and micro-scale distances causes an attraction between the two. This effect, known as the Casimir effect, was first predicted by H. Casimir in 1948[1] for two infinitely thin perfectly conducting plates (with infinite plasma frequency) in vacuum, at zero temperature. The corresponding force, per unit area, is expressed as $F_c = -\frac{\pi^2 \hbar c}{240 d_0^4}$, where the minus sign specifies the attractive nature of the force, d_0 denotes the separation distance between the plates, and the rest are universal constants. This interaction can be considered instantaneous, known as van der Waals (vdW) force[2] at short separation distances, or retarded, when the finite speed of light becomes relevant, as expanded by Casimir and Polder[3] for large distances between the objects. A decade after Casimir's prediction, Lifshitz and co-workers extended the theory[4,5] at finite temperature to bodies of arbitrary shape immersed in fluids different from vacuum, and unconstrained optical and magnetic properties, parameters that, in addition to the separation distance between the bodies, modulate the so called Casimir-Lifshitz force, F_{C-L}. Over the last two decades, the topic of Casimir physics has flourished, as fundamental questions and technological applications remain irresolute and/or unexploited. Evidence of the latter are the excellent review and perspective articles on F_{C-L}[6,7] that guide for the application of the extended Lifshitz theory to real[8] and novel materials,[9,10] including nanocomposites,[11] and which survey current progress and applications to nanophotonics, nanomechanics, chemistry,[12] and nanotechnology.[13] Not only that, dynamic effects[14-16] and quantum friction[17-23] are currently hot topics in the

V. Esteso
European Laboratory for Non-Linear Spectroscopy (LENS)
Via Nello Carrara 1, Sesto Fiorentino 50019, Italy

V. Esteso
Departamento de Física de Materia Condensada
ICMSE-CSIC
University of Seville
Apdo. 1065, Sevilla 41080, Spain

The ORCID identification number(s) for the author(s) of this article can be found under https://doi.org/10.1002/apxr.202300065

[+]Present address: Instituto de Ciencia de Materiales de Madrid, ICMM-CSIC, C/Sor Juana Inés de la Cruz, 3, Madrid 28049, Spain

D. Frustaglia
Departamento de Física Aplicada II
University of Seville
Sevilla E-41012, Spain

S. Carretero-Palacios[+]
Departamento de Física de Materiales
Universidad Autónoma de Madrid
Madrid 28049, Spain
E-mail: sol.carretero@uam.es sol.carretero@csic.es

S. Carretero-Palacios[+]
Instituto de Ciencia de Materiales Nicolás Cabrera (INC)
Universidad Autónoma de Madrid
Madrid 28049, Spain

H. Míguez
Institute of Materials Science of Seville
Consejo Superior de Investigaciones Científicas (CSIC)-Universidad de Sevilla (US)
Seville 41092, Spain
E-mail: h.miguez@csic.es

field of Casimir science and quantum fluctuation related phenomena.

In nature, such pervasive effect arising from zero-point fluctuations of quantum fields governs, for example, the adhesion of gecko's feet to surfaces,[24,25] or determines whether wetting occurs between a surface and a liquid.[26] It is responsible, for instance, for the unusual ice wet behavior,[27] when a thin liquid layer forms on ice at the triple point. The formation of such thin liquid layer has key environmental implications, affecting for example the charging of thunderclouds[28–30] and frost heave,[31,32] and it may also serve as a habitat for life, including icy moons and exoplanets.[33–38] Not only that, this transversal effect has been proposed as responsible for the possible evaporation of black holes through Hawking radiation.[39] Along these lines, the thermodynamic equivalent of F_{C-L}, the critical Casimir force[40–42] caused by the thermal fluctuations in the local composition of a binary fluid close to its critical point, acts for instance inside cellular membranes on the proteins, allowing the latter to communicate with one another and stimulating cells' responses to allergens.[43] Similarly, because of the significant strength of F_{C-L} at nano- and micro-scale distances, strong efforts have been devoted to control it in NEMS and MEMS,[44–51] as, together with electrostatic forces, it is at the root of their malfunction when some of their component parts rub against each other, or stick together, a phenomenon called Casimir pull-in.[52] In this context, the magnonic Casimir effect has been recently demonstrated in ferrimagnets.[53]

A fascinating result of the extended theory by Lifshitz and collaborators[4,5] is the prediction of a repulsive force under specific conditions, contrary to the antecedent Casimir effect.[1] This result enables the possibility of fine-tuning and controlling the intensity and nature of such force at the nano-scale, making it a subject of both fundamental interest and technological relevance. However, accurately measuring F_{C-L} presents various challenges.[54] These include i) minimizing the effect of surface roughness of the interacting materials,[55,56] which becomes important at distances considerably shorter than the root-mean-square roughness, ii) considering the influence of finite compliance of the interacting materials,[57] iii) accounting for the presence of patch electrostatic potentials,[58–62] or iv) addressing non-desirable electrostatic forces, F_{el}, which may cover up F_{C-L} as it dominates at micro- and nano-scales.[63] When a fluid is present, the interaction is mediated by the electrostatic interaction resulting in the double-layer force. The Poisson-Boltzmann approximation is often used to calculate it between two surfaces with their respective ion layers, by describing the electrostatic potential. The double-layer force per unit area can be obtained from the limit of small potentials.[64,65] Bearing in mind such experimental demands, and the technological needs to accurately determine this small dispersion force at very short separation distances, it is not surprising the struggles and efforts that were dedicated to measure the attractive F_{C-L} with high accuracy for the first time. The experiments conducted by Lamoreaux[66] in 1997, employing a torsion balance, and the subsequent ones by Mohideen[67–71] using an atomic force microscope (AFM), are widely regarded as the pioneering experimental assessments of attractive F_{C-L}. However, these results came to an agreement of 5% with the theoretical predictions. A series of more accurate measurements followed using a micromachined torsional device,[72,73] but it was not until 2005 that the attractive F_{C-L} was verified precisely for the first time in a collection of experiments performed by Decca et al.[74–79] By employing a micromechanical torsional oscillator, isoelectronic differential force measurements at submicron separations were reported between a gold (Au)-coated probe and two Au-coated films, made out of Au and Germanium (Ge), and variations of the same. Shortly thereafter, and although the repulsive nature of van der Waals force (non-retarded limit of F_{C-L}) was experimentally observed two decades before,[80,81] the first experimental evidence of repulsive F_{C-L} was proved by Munday et al. in 2009.[82] Specifically, a Au-coated polystyrene (PS) sphere attached to an AFM cantilever was enclosed within a bromobenzene-filled cell for force measurements, facing a silica (SiO_2) plate. Ever since Casimir's and Lifshitz's predictions, a plethora of approaches to controllably tune[83,84] and measure[85–91] F_{C-L} have been realized, including the experimental observation of the thermal Casimir force,[92] i.e., that arising from thermal rather than quantum fluctuations of the EM field at finite temperature. To fine tuning F_{C-L}, some strategies cover nanostructuring the surface of the interacting materials,[93–95] modifying the dielectric properties of materials under external means,[96–101] changing the carrier density,[87,102] or employing external magnetic fields.[103] Other approaches consider the use of hyperbolic,[104,105] chiral,[106,107] magnetic,[108] magnetodielectric,[109] or 2D materials[110,111] like the graphene family,[112–115] as well as the mixing of various materials in finite multilayer architectures,[116–120] or composites.[121–123] On the road to quantitative determine F_{C-L}, several outstanding technological approaches have been explored. These include, as previously mentioned, the use of a micromechanical torsional oscillator or a cantilever,[124] even for a three-body system.[125] More recently, optical tweezers have been utilized for this purpose.[126–128] All of them are commonly employed in the sphere-plane or sphere-sphere geometries, as attaining perfect alignment and parallelism between plates is an arduous task that might compromise the outcome of the results. An alternative method consists of the quantum trapping of one of the interacting objects[129–141] assisted by F_{C-L}. As a result of the forces acting on it, the object is suspended over the other, achieving a state of balance. This approach is especially useful for planar plates, as the forces exerted on the suspended film inherently promote parallelism between the two plates. This solves the longstanding challenge of measuring forces in plane-parallel systems. When metallic plates interact in this way, they form an optical resonator,[120–124] paving the way for exploring novel physics and chemistry at the nano-scale.[142,143] Additionally, this technique allows for the indirect measurement of F_{C-L} using spectroscopic methods,[144] which provides a new avenue for studying the behavior of quantum and photonic systems. This review article provides a comprehensive summary of the latest findings in F_{C-L} optical resonator schemes, which offer an exciting opportunity to investigate nano-scale physics. Furthermore, we examine the potential of this technology to be applied in various technological devices, such as microfluidic devices and bio-NEMS and MEMS, as well as in fields like strong coupling, polaritonic chemistry, photo-chemistry, sensing, or metrology, among others.
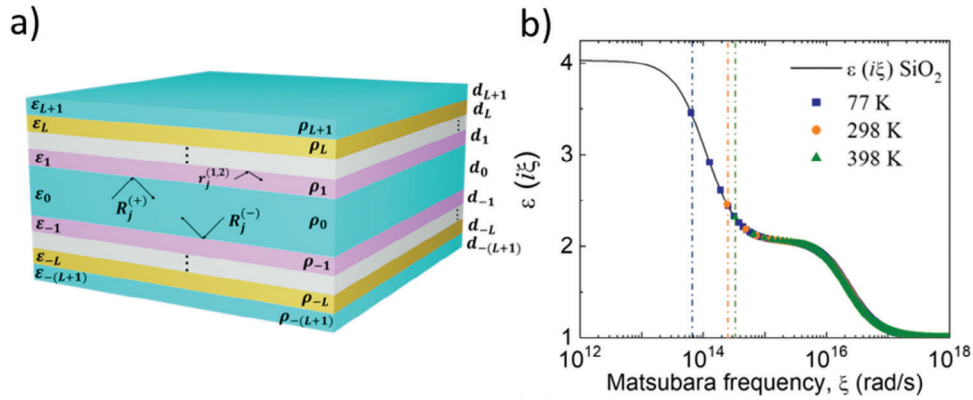
Figure 1. a) Scheme of a mutilayer structure of an arbitrary number of layers for the F_{C-L} calculation. Each layer is characterized by its dielectric function ϵ_l, density ρ_l, and thickness d_l. $l = 0$ stands for the material layer mediating the interaction between top and bottom layers. $R_j^{(\pm)}$ are the multiple Fresnel coefficients on the top (+) and the bottom (-) interfaces of the material mediating the interaction. b) Dielectric permittivity of SiO_2 evaluated at Matsubara frequencies. Vertical lines correspond to the first non-zero frequency considered in the integration in $\epsilon(i\xi_n)$ through $i\xi_n = i\frac{(2\pi k_B T)n}{\hbar}$ in the calculation of F_{C-L}, contingent upon the temperature under evaluation. Specific temperatures correspond to T = 77 K (blue squares), 298 K (yellow circles), and 398 K (green triangles). This selection serves as an illustration of the behavior in both low-temperature systems and room temperature systems, along with fluctuations occurring around the latter.

1.2. Repulsive Casimir-Lifshitz Force and Quantum Trapping

The F_{C-L} expression can be derived through various approaches, such as quantum statistical physics, thermal quantum field theory, scattering theory, and more.[116,119,145–150] One of the initial approximations involves solving Maxwell's equations for macroscopic materials, computing the Maxwell stress tensor ($\mathcal{T}$) using the fluctuation-dissipation theorem, and then taking the average of the zz-component, denoted as $\langle \mathcal{T}_{zz} \rangle$, expressed in terms of Green functions. Lifshitz originally obtained the closed-form expression for the plane-parallel configuration, known as the Lifshitz formula, using this method. Alternatively, another common procedure considers the fully quantum nature of EM fields. In this approach, the energy difference inside and outside the cavity formed by two interacting bodies is determined by calculating the eigenvalues of the allowed modes within it. Regardless of the chosen approach, the F_{C-L} in the plane-parallel configuration takes on different forms depending on the evaluation temperature (T = 0 K or T > 0 K) and the plane of frequency integration. To avoid rapid oscillations taking place in the integrand when computing F_{C-L} in the real axis, a closed integral in the complex plane can be performed.

To provide an expression for F_{C-L} in a general multilayer scheme, let us consider the system displayed in **Figure 1a**. In it, layers are symmetrically piled up above and below the material that mediates the interaction between top and bottom layers. Each layer is labeled by index $l = -L, ..., L$ (with $L = 1, 2, ...\infty$), being $l = 0$ the central material, and positive and negative indexes accounting for upper and lower layers, respectively. The total number of layers is given by $2L+1$, and the two semi-infinite materials enclosing the system are excluded in this numeration. Each layer is described by its dielectric function ϵ_l, density ρ_l, and thickness d_l, being $d_{(L+1)}$ and $d_{-(L+1)}$ equal to infinite as they account for semi-infinite materials. In the realm of the complex plane at finite temperature, the F_{C-L} in a general multilayer system depends upon numerous factors. This includes the multi-

ple Fresnel coefficients associated with both the upper ($R_j^{(+)}$) and lower ($R_j^{(-)}$) surfaces of the mediating layer, which are expressed as an iterative function of the corresponding simple Fresnel reflection coefficients of the interfaces above and below such material, r_j (as displayed in Figure 1a). These coefficients take on distinct values for transverse magnetic (TM) and electric (TE) polarizations (j = TM, TE)

$$r_{TM}^{(l,l')}(n, \mathbf{k}_\perp) = \frac{\epsilon_n^{(l')} k_n^{(l)} - \epsilon_n^{(l)} k_n^{(l')}}{\epsilon_n^{(l')} k_n^{(l)} + \epsilon_n^{(l)} k_n^{(l')}} \tag{1.a}$$

$$r_{TE}^{(l,l')}(n, \mathbf{k}_\perp) = \frac{k_n^{(l)} - k_n^{(l')}}{k_n^{(l)} + k_n^{(l')}} \tag{1.b}$$

In the above expression, the dielectric functions are evaluated at the so-called Matsubara frequencies, $i\xi_n$, after a Wick rotation,

$$\epsilon(i\xi_n) = 1 + \frac{2}{\pi} \int_0^\infty \frac{\omega \epsilon''(\omega)}{\omega^2 + \xi_n^2} d\omega \tag{2}$$

where ω denotes the light frequency, $\epsilon''(\omega)$ the imaginary part of the complex permittivity $\epsilon(\omega) = \epsilon'(\omega) + i\epsilon''(\omega)$, $i\xi_n = i\frac{(2\pi k_B T)n}{\hbar}$, with $n = 0, 1, 2, 3, ...$, and T the temperature.

Also, the wavevector inside the liquid layer has two components: $\mathbf{k}_\perp$ is the projection of the wave vector on the interface of the layers, and k_l^n is perpendicular to the layer's interface, with $k_l^n = k_l(i\xi_n, k_\perp) = [\mathbf{k}_\perp^2 + \epsilon^{(l)}(i\xi_n)\frac{\xi_n^2}{c^2}]^{\frac{1}{2}}$. $\mathbf{K} = (\mathbf{k}_\perp, k_n^{(0)})$, $k_n^{(l)} = [\mathbf{k}_\perp^2 + \frac{\epsilon_n^{(l)}\xi_n^2}{c^2}]^{\frac{1}{2}}$. Finally, $R_j^{(\pm)}$ take the form:

$$R_j^{(\pm)}(n, k_\perp) = \Gamma_{l=0}^{(\pm)}(n, k_\perp) \tag{3}$$

**ADVANCED
SCIENCE NEWS**

www.advancedsciencenews.com

**ADVANCED
PHYSICS
RESEARCH**
Open Access

www.advphysicsres.com

where the $\Gamma_l^{(\pm)}$ functions are expressed as:

$$\Gamma_l^{(\pm)}\left(n, k_\perp\right) = \frac{r_j^{(l,l\pm1)} + \Gamma_{l\pm1} e^{-2k_{l\pm1}^n d_{l\pm1}}}{1 + r_j^{(l,l\pm1)} + \Gamma_{l\pm1} e^{-2k_{l\pm1}^n d_{l\pm1}}} \qquad (4)$$

Notice that, for the interface of the semi-infinite materials, the above expression becomes $\Gamma_L^{(+)} = r_j^{(L,L+1)}$ and $\Gamma_{-L}^{(-)} = r_j^{(-L,-(L+1))}$, for the upper and the lower interfaces, respectively, since the infinite thicknesses $d_{(L+1)}$ and $d_{-(L-1)}$ in the negative exponential makes zero the rest of terms.

Finally, F_{C-L} in the complex realm can be expressed as:

$$F_{C-L}\left(i\xi, T > 0\right)$$

$$= -\frac{k_B T}{\pi} \sum_{n=0}^{\infty}{}' \int_0^\infty k_0^n k_\perp dk_\perp \sum_{j=TE,TM} \left[\frac{e^{2k_0^n d_0}}{R_j^{(+)} \cdot R_j^{(-)}} - 1\right]^{-1} \qquad (5)$$

Importantly, in the summation, the presence of a "prime" signifies that the $n = 0$ term must be adjusted by a factor of 1/2. Note that the above expression applies for realistic materials, at low temperatures, and short separation distances. However, at elevated temperatures within the framework of non-relativistic quantum electrodynamics, which includes quantum and thermal fluctuations of both matter and the field, a different expression should be used.[151,152]

Equation (5) considers the effect of temperature through the integration of a diverse number of Matsubara frequencies, depending on the working temperature. Figure 1b shows the dielectric function of SiO_2 evaluated at Matsubara frequencies. To offer a representative example, we have included the specific count of Matsubara frequencies utilized in the computation at temperatures of T = 77 K, 298 K, and 398 K. This selection of temperatures serves as an illustration of the behavior in both low-temperature systems and room temperature systems, along with fluctuations occurring around the latter. The vertical lines on the graph correspond to the first non-zero frequency considered in the integration in $\epsilon(i\xi_n)$ in Equation (2) in the calculation of F_{C-L}, contingent upon the temperature under evaluation. As the temperature increases, the summatory converges for a lower number of Matsubara frequencies.

Expressions for F_{C-L} at T = 0, and alternative ones to compute the force in the real axis, can be obtained elsewhere.[147]

The ability to control repulsive F_{C-L} at the nano-scale presents a multitude of potential applications, including contact-free nanomachines, ultrasensitive force sensors, nano-scale manipulation, and controlled self-assembly. Two paths can be taken to achieve repulsive F_{C-L}. The first involves designing the geometry of the interacting objects, such as through microstructuring their surfaces[153,154] or by employing anisotropic dipolar bodies.[155] The second path relies on the relationship between the dielectric functions of the interacting materials, where a necessary condition (but not sufficient) for realizing repulsive F_{C-L} between the objects must be fulfilled, and is expressed as,[5]

$$\varepsilon_1 (i\xi) > \varepsilon_0 (i\xi) > \varepsilon_2 (i\xi) \qquad (6)$$

where subscripts 1 and 2 denote the bodies that interact through an intermediate fluid, 0. This condition must be satisfied over a wide frequency range, making the choice of materials a complex task. Note that the integral in Equation (2) is done over an infinite frequency range, which strongly reduces the choice of materials to be used as such information is usually experimentally limited. To overcome this problem, the macroscopic dielectric function of a material is alternatively determined through the Density Functional Theory (DFT),[132,156] Drude-Lorentz models,[157] or the so-called generalized plasma-like dielectric permittivity.[158] Equation (1) reveals that F_{C-L} will always be attractive if the two interacting objects are made of the same material, or if two objects of different composition are separated by air or a vacuum. To achieve repulsive F_{C-L} using real materials (i.e., those with well-known and characterized optical constants, including all dissipative wavelengths), a fluid with a permittivity greater than that of one of the interacting bodies is required. Compared to a vacuum-separated configuration, a liquid environment allows for modification of both the magnitude and sign of F_{C-L}, with the possibility of switching from attractive to repulsive (and vice versa) through the separation of the bodies. This is a perfect scenario for designing repulsive forces in microfluidic devices, and bio-NEMS and MEMS, in which F_{C-L} might affect their mechanical properties, and ultimately, their performance. In the case of biosensors, for example, this effect extraordinarily impacts the sensitivity and operation of actuated ultra-small detectors.[159] Recent theoretical proposals have suggested engineering Casimir interactions in vacuum to achieve repulsive F_{C-L} by designing near-zero-epsilon metamaterials[160] in plates, or broadband perfect magnetic conductor metamaterials[161] in a sphere-plate arrangement.

Until very recently, only the use of a cantilever had been proven successfully to measure F_{C-L} of repulsive nature. In such technique, the movement of the two interacting macroscopic bodies is restricted as they are active components for measuring the force. However, quantum trapping offers a passive alternative for determining repulsive F_{C-L} by examining the levitation of a free-moving object, balanced by mainly repulsive F_{C-L}, gravity (F_g), and buoyancy (F_b). In addition to the aforementioned forces, other forces may come into play. F_{el}, as previously noted, can typically be neutralized by introducing monovalent salts into the surrounding fluid. The Stefan force (F_S), also known as the viscous adhesion between rigid plates, describes the force per unit time needed to separate the parallel plates within a viscous fluid. As this is a force associated to the dynamics of the system, it can be overlooked when the system reaches equilibrium. While conducting spectroscopic experiments, external light sources generate radiation pressure (F_{RP}), yet unless high-power lasers are employed, the impact of white lamps can be disregarded. Likewise, when the entire levitating film is fully immersed and there is no interface between two fluids, the surface tension is absent. The fact that the application of this quantum trapping strategy can be extended to plates puts it in the spotlight since, in comparison to the sphere-sphere or sphere-plane geometries, this fully planar configuration produces the highest intensity force. Indeed, theoretical schemes on stable quantum levitation of objects in fluids under the action of repulsive F_{C-L} were initially proposed[130–136] for planar plates and nanoparticles, considering materials whose optical constants are known for a sufficiently broad frequency

**ADVANCED
SCIENCE NEWS**

www.advancedsciencenews.com

**ADVANCED
PHYSICS
RESEARCH**
Open Access

www.advphysicsres.com

range characterizing all dissipation wavelengths. Among them, silicon (Si), polystyrene (PS), SiO_2, Teflon (PTFE), Au, or lithium niobate ($LiNbO_3$), immersed in ethanol, bromobenzene, water, toluene, or glycerol, stand out because of their ease of processing and functionalization (thus avoiding the possible appearance of non-desirable F_{el}), and because they have densities that allow balancing the sum of forces acting on the levitating object.

Like optical tweezers,[162] the technique par excellence for applying well-defined forces and torques as well as for manipulating nano- and micro-scale objects non-invasively,[163–166] quantum trapping of objects at the nano-scale under the influence of Casimir science enables the application of precise forces and torques[167–169] that can be much stronger than the trapping force in optical tweezers. Moreover, this quantum effect expands the scope of physical phenomena that can be investigated, such as the diffusion of 2D objects that are confined in a plane due to trapping conditions. This capability would allow the investigation of the stability and self-assembly of colloids in the absence of a substrate, for instance. In this regard, a novel concept based on the quantum trapping of a metallic plate shaping an optical resonator, or Fabry-Pérot cavity, has been recently come into view.[120–124] Optical resonators consist of arrangements of mirrors that trap light. Confined light modes of a given frequency inside such cavity reflect multiple times, giving rise to characteristic light reflectance spectra displaying sharp features at resonant wavelengths. Within the quantum trapping framework, one of the metallic plates levitates under the influence of F_{C-L} over the other at nano-scale distances, creating a perfect scenario for indirectly measuring F_{C-L} with spectroscopic techniques. Through such avenue applied to planar plates, a far-field measurement enables to observe physical phenomena occurring at the nano-scale, not even accessible through specialized microscopes. This trapping force provided by quantum fluctuation–induced EM fields at finite temperature is passive, without any external energy input, which leads to contact-free nanomechanical systems and controlled self-assembly, amongst others, positioning itself as a new platform for exploring physics at the nano-scale[125,126] as well as to harness the technological potential of Casimir phenomena in fields such as strong coupling,[170] chemistry,[171] polaritonic chemistry,[172,173] photo-chemistry,[174,175] or metrology,[134] among others. The above strategy is in its early or proof-of-principle stage, a fact that provides ample room for future research. Here, we review recent proposals and designs of Casimir-Lifshitz force-based optical resonators and advise potential applications in contact-free nanomachines, ultrasensitive force sensors, nano-scale manipulations, or controlled self-assembly.

2. Theoretical Proposals

In the context of the aforementioned Fabry-Pérot cavity scheme, which involves a pair of metallic plates forming an optical resonator with one of them suspended and influenced by F_{C-L}, designers are currently experimenting with spectroscopic techniques to indirectly measure F_{C-L}. In addition to validating the effectiveness of the proposed designs, these experiments conducted over the past four years not only provides valuable insights into F_{C-L}, but also paves the way for novel scientific discoveries and possibilities. In theoretical proposals based on this

concept, repulsive F_{C-L} is demonstrated in metallic plates forming a nano-scale optical resonator through an appropriate stratification of the inner dielectric media. At resonant wavelengths, $\lambda_r = \frac{2\tilde{N}d\cos(\theta)}{m}$ (with $\tilde{N}$ the refractive index between the mirrors, d the size of the optical resonator cavity, θ the angle of the incident light, and m the order of diffraction), sharp minima in reflectance emerge and from their spectral position the distance d at which one of the mirrors levitates can be determined. In this kind of scheme, it is mandatory to have a precise knowledge of the measured layer thickness of all materials in the stratified cavity, and to achieve perfect alignment between the parallel plates to maximize the precision of the estimated equilibrium distance. In a stable quantum trapping position, a total repulsive (positive) force is found at short separation distances, which changes to be attractive (negative) at larger ones. In this situation, any slight deviation from that stable position will lead to a force pointing to the equilibrium position. On the other hand, when a total attractive force governs at short distances, and a repulsive one is found at larger separations, the equilibrium position is unstable and any deviation from it will provoke that the film will either get attached to the substrate or float.

In a recent study,[138] we presented a novel design in which an Au substrate coated with a variable thickness SiO_2 layer serves as one of the mirrors in an optical resonator architecture. Separately, a second mirror, formed by an Au-PS bilayer, is immersed in glycerol and placed above the first mirror. Through the balance of all the considered forces acting on the system, including F_{C-L}, the second mirror levitates at a stable equilibrium position (see inset in **Figure 2a**). In contrast to alcohols suffering from evaporation, glycerol presents stable dissipation properties with potential applications in promising technologies based on such levitation effect. The rational selection of materials composing the simulated system cover three main requirements to eventually measure repulsive F_{C-L}, namely, i) they can be prepared with exceptional optical quality, ii) a fine tuning of their thicknesses is experimentally feasible (from a few tens of nanometers to several hundreds of nanometers) to sustain optical modes at visible frequencies, and iii) repulsive F_{C-L} is experienced at short separation distances between the plates.

Figure 2a displays the dielectric function evaluated at Matsubara frequencies for the selected materials that fulfill the condition $\varepsilon_{Au}(i\xi) > \varepsilon_{Glycerol}(i\xi) > \varepsilon_{SiO_2}(i\xi)$ over a broad frequency range. Figure 2b exhibits the logarithmic scale force acting on the levitating Au-PS mirror over a SiO_2-coated Au substrate as a function of the separation distance between the two mirrors that form the optical resonator, demonstrating the exemplary behavior of the design. This setup can avoid potentially undesirable F_{el} due to the presence of salts in the liquid medium. In this levitation scenario at equilibrium, we consider the impact of various forces (per unit area). The gravitational force ($F_g = (\rho_{Au} \cdot d_{Au} + \rho_{PS} \cdot d_{PS}) \cdot g$), determined by the densities (ρ_{Au} and ρ_{PS}) and thicknesses (d_{Au} and d_{PS}) of the Au and PS layers, is calculated as 0.021 N·m^{-2}. The buoyant force ($F_b = \rho_{Gly} \cdot (d_{Au} + d_{PS}) \cdot g$), dependent on the density of glycerol (ρ_{Gly}) and the total thickness of both layers, is found to be 0.019 N·m^{-2}. To assess the influence of double layer forces in our system, we calculate the F_{el} using the Poisson-Boltzmann method. The total free energy per unit area within the electrolyte, situated between planar surfaces,
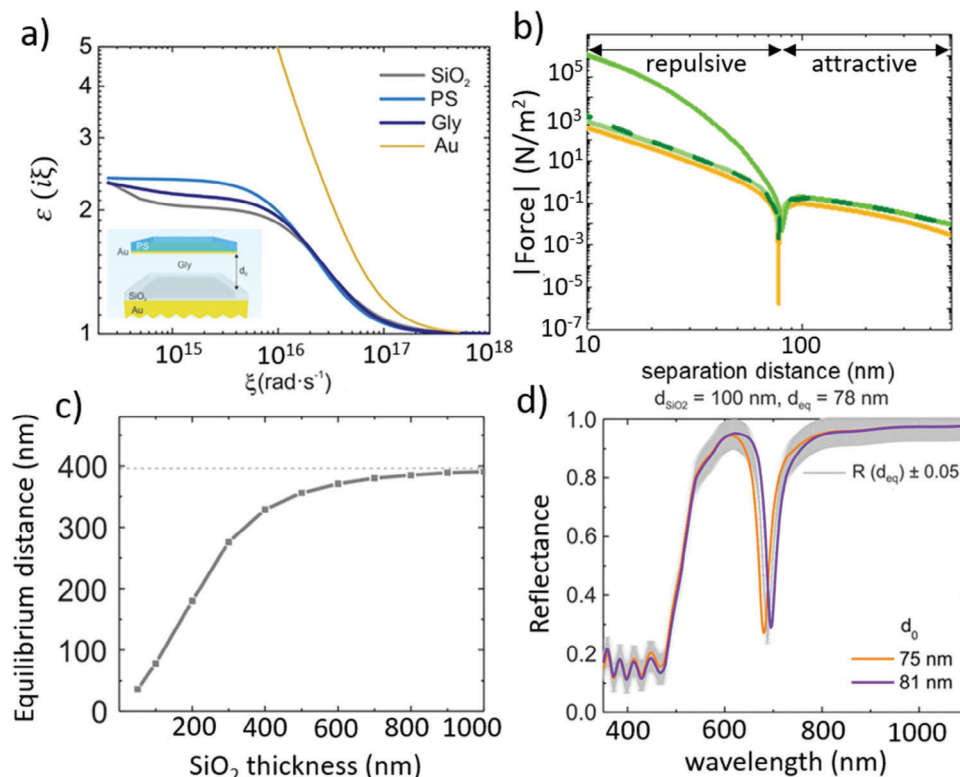
2300065 (5 of 14)

Figure 2. a) Dielectric permittivities evaluated at Matsubara frequencies, $\epsilon(i\xi)$, for the materials composing the optical resonator proposed displaying levitation due to the balance of repulsive F_{C-L}, gravity and F_b: SiO$_2$ (in gray), PS (in blue), glycerol (in navy), and Au (in yellow). Inset: scheme of the optical resonator architecture. It consists of a SiO$_2$-coated Au substrate with a suspended Au/PS bilayer on top. The whole arrangement is immersed in glycerol. The glycerol layer thickness between the substrate and the bilayer is denoted by d_0. In the case of levitation, $d_0 = d_{eq}$. b) Modulus of the dominant forces (in logarithmic scale) acting on an exemplary levitating system (consisting on a 100 nm SiO$_2$ coating layer, and a Au/PS bilayer of 30 and 1500 nm thickness, respectively), as a function of the separation distance. F_{C-L} is shown in yellow color, and $F_{C-L} + F_b + F_{el}$ assuming either F_{el} = 0 or the addition of a monovalent salt with concentrations 3 and 60 mM are shown in light green, dark green, and dashed green colors, respectively. c) For diverse optical resonator designs, and assuming $F_{el} = 0$, equilibrium distance as a function of the SiO$_2$ coating layer thicknesses (with d_{PS} = 1500 nm and d_{Au} = 30 nm fixed) conforming the optical resonator arrangement. d) Resulting reflectance at normal incidence for a system displaying stable levitation corresponding to the set of parameters d_{PS} = 1500 nm, d_{Au} = 30 nm, $d_{glycerol} = d_{eq}$ = 78 nm, and d_{SiO_2} = 100 nm, with an assumed error in the reflectance of ±0.05 (in gray). Also, for separation distances of $d_{glycerol} = d_0$ of 75 nm and 81 nm, results are shown in orange and purple colors. These latter results would correspond to systems out of equilibrium. Adapted with permission.[138] Copyright 2019 American Chemical Society.

is determined based on the electrostatic potential and ion concentration profiles. Subsequently, this free energy is transformed into an electrostatic force per unit area[65,64] under the assumption of small potentials, having: $F_{el} = \frac{2}{\epsilon\epsilon_0} \frac{(\sigma_1^2 + \sigma_2^2 + \sigma_1\sigma_2(e^{K_D d_0} + e^{-K_D d_0}))}{(e^{K_D d_0} - e^{-K_D d_0})^2}$, with σ_1 and σ_2 representing the surface charge of each semi-infinite surface and both equal to -0.05 C m^{-2} as a representative value for monovalent salts in water,[176,177] such NaCl and KCl at pH = 7, ϵ signifying the dielectric constant of the surrounding medium in which the electrolyte is dissolved, ϵ_0 as the vacuum permittivity, and K_D being the reciprocal of the Debye length (l_D), which is defined as follows: $K_D = \frac{1}{l_D} = \sqrt{\frac{2(Ze)^2 p}{\epsilon k_B T}}$. Here, Z and p represent the valence and the concentration per unit volume of the salt ions, respectively, with e denoting the elementary charge. Regarding the effect of radiation pressure in such experiment, its upper limits, assuming perfect reflection ($F_{RP} = 2 I/c$) or perfect absorption ($F_{RP} = I/c$) of white light, are 0.007 N m^{-2} and 0.003 N m^{-2}, respectively. Such estimations are done considering I the irradiance per unit area of a 1 mW of light power im-

pinging on an area 100 μm x 100 μm, and c the speed of light. Such intensity of the radiation pressure barely modifies the equilibrium distance in just a few nanometers. However, the actual radiation pressure is lower due to white light transmission. In a dynamic system out of equilibrium, based on Stefan's theory for the viscous adhesion, the bilayer's displacement time from 100 to 1 μm from the substrate is estimated at ≈4 h, while moving only 5 nm (from 75 to 80 nm) closer to the equilibrium position takes ≈70 days. These estimations are done according to the Stefan theory[178] rewritten by Bikerman[179] which describes the Stefan adhesive force per unit area, $F_S = -\frac{dh}{dt} \cdot \frac{3}{2}\eta \cdot \frac{R^2}{h^3}$, between two rigid disks of radius R, separated a distance h, within a fluid of viscosity η.[180] In our specific context, we assume a representative radius of $R \approx 5$ mm, which is typical for standard gold flakes,[140,141] and employ a viscosity value of $\eta = 1.5$ Pa·s^{-1} for glycerol at 293 K. We consider two different constant forces that counteract F_S: 0.002 N·m^{-2} for large separation distances and 0.0001 N·m^{-2} for short separation distances. These forces account for the equilibrium achieved through the balance

**ADVANCED
SCIENCE NEWS**

www.advancedsciencenews.com

**ADVANCED
PHYSICS
RESEARCH**
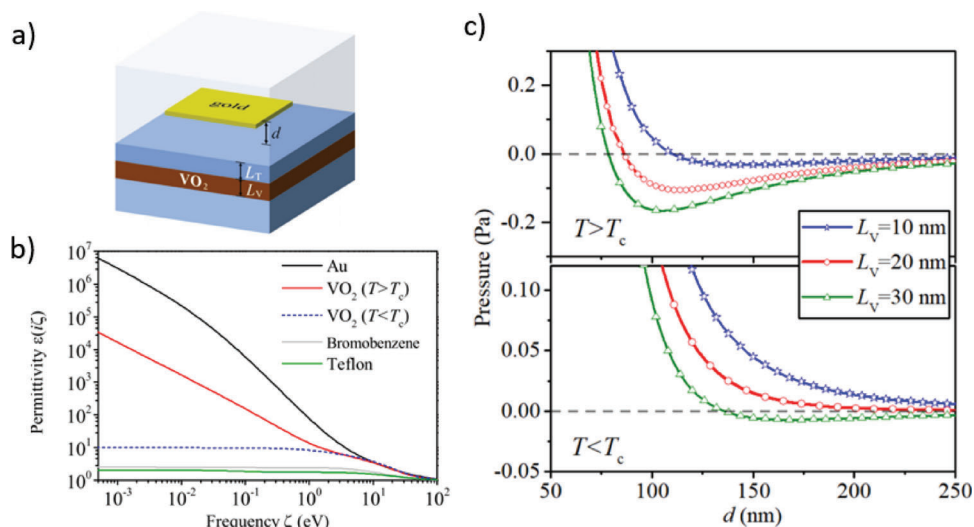Open Access

www.advphysicsres.com

Figure 3. a) Schematic of the type of architectures proposed: a gold nanoplate is suspended in bromobenzene over a PTFE coated VO$_2$ slab, both of variable thickness, on top of a PTFE substrate. b) Dielectric permittivities evaluated at Matsubara frequencies, $\epsilon(i\xi)$, of Au, VO$_2$ (above and below the critical temperature, T_c), bromobenzene, and PTFE. c) For thin VO$_2$ thicknesses (10, 20, and 30 nm), F_{C-L} as a function of the separation distance between a gold nanoplate and a PTFE /VO$_2$/ PTFE multilayers. The thicknesses of PTFE and Au slabs are fixed to 45 and 40 nm, respectively. Top panel corresponds to temperatures $T > T_c$ (i.e., to the metallic phase of VO$_2$), and bottom panel to $T > T_c$ (i.e., to the insulating VO$_2$ phase). Adapted with permission.[139] Copyright 2020 American Physical Society.

of gravity, buoyancy, and a nearly negligible net force near the equilibrium position, respectively. It is worth noting that the viscosity of glycerol experiences a rapid decrease as the temperature rises. For instance, at 333 K, its viscosity is 0.1 Pa·s^{-1}, and it eventually matches that of water (0.001 Pa·s^{-1}) at 393 K. At such low viscosity, the displacement time of the same system is drastically reduced, taking just 9 s to displace the bilayer film from 100 to 1 mm from the substrate, and at equilibrium, 1 h and 15 min. Therefore, if needed, the dynamics of the system could be accelerated significantly by elevating the temperature by several tens of degrees Kelvin. Furthermore, once the system achieves equilibrium under these elevated temperature conditions, it could be effectively "dynamically frozen" by cooling it back to room temperature. This cooling process would reintroduce a higher degree of viscous adhesion, making it less likely for the system to easily depart from equilibrium. By adjusting the thickness of the PS, Au, or SiO$_2$ layers, the equilibrium distance at which the Au-PS mirror levitates can be finely tuned over a range of several hundred nanometers (Figure 2c). The model demonstrates that highly relevant information about the properties and forces acting on the system can be extracted with the experimentally attainable Q-factors of this design. Precise determination of the levitating position is achievable for Q-factors > 150. However, for Q-factor values below this threshold, the impact of various error sources resulting from misalignment, surface roughness, measurement precision, F_{el}, layer thickness inaccuracy, etc., cannot be identified. As shown in Figure 2d, reflectance measurements of an optical resonator with a Q-factor of 164 in levitation state are superimposed with a grey line representing variations of ± 5% that take into account the above-mentioned error sources. Furthermore, utilizing the same spectroscopic technique on the levitating system allows for the detection of temperature variations, including more substancial changes spanning several tens of degrees. In the context of this scenari, it is estimated that a change

in the equilibrium distance occurs at a rate of approximately 0.13 nm per Kelvin, in the vecinity of room temperature. While our system may not offer high precision, it can effectively discern alterations on this scale. For instance, changes from 25ºC to 35ºC result in noticeable adjustments in the separation distance, underlining the system's ability to resolve temperature fluctuations of this order. Also, it should be remarked that the possibility to determine the equilibrium distance in a non-invasive way, as the Casimir-Lifshitz optical resonators allow, expands the range of physical phenomena that can be explored, such as the diffusion of objects in 2 dimensions (2D) under trapping conditions.

An alternative theoretical approach brought by Ge et al.[139] enables tunable trapping by external stimuli. Their proposal involves the incorporation of a phase-change material, which enables the fine tuning of both the intensity and direction of F_{C-L} between a levitating nanoplate and a layered structure by varying the thickness and the phase (metallic or insulating) of the phase-change material. Moreover, the capability of releasing the nanoplate from the levitated state is demonstrated by thermal methods in a fluid environment. Their strategy has the virtue of allowing the tuning of the trapping once the devices are fabricated. The proposed design involves trapping Au or PTFE nanoplates in bromobenzene using a substrate made of vanadium dioxide (VO$_2$) sandwiched between PTFE layers (**Figure 3a**). The thicknesses of the slabs cover a range of a few tens to several hundreds of nanometers, making the design potentially realizable. VO$_2$ undergoes a metal-to-insulator transition at a critical temperature of 340 K, resulting in a dramatic variation of its dielectric function. The relative relationship between the dielectric permittivity of all the interacting materials (Figure 3b) and the penetration of the field is key to modulating and controlling the trapping or release of the flakes by varying either the temperature (which defines the matter phase of the VO$_2$ material) or the thicknesses of the materials in the stratified

2300065 (7 of 14)

**ADVANCED
SCIENCE NEWS**

www.advancedsciencenews.com

**ADVANCED
PHYSICS
RESEARCH**

www.advphysicsres.com

Table 1. Experiments based on the F_{C-L} in the plane-parallel geometry which lead to the formation of an optical resonator, due to the trapping of a gold flake in a fluid over a reflective substrate.

	a)	b)	c)
System sketch			
Repulsive interaction	Casimir-Lifshitz force	Electrostatic force	Critical Casimir force
Cavity size measurement	Spectroscopy	Spectroscopy	2D flake diffusion or Spectroscopy
Tuning method	Coating thickness	Ligand concentration 0.116 – 1.425 nm Laser radiation pressure Silica coating thickness	Temperature 33–34 °C
Tunable cavity range	75–150 nm	84–160 nm	100–200 nm
Ref.	[137]	[140]	[141]

VO$_2$ substrate (which determines the reach of the interaction), as shown in Figure 3c. Whereas the dielectric functions of Au, bromobenzene, and PTFE fulfill the condition $\epsilon_{Au}(i\xi) > \epsilon_{bromobenzene}(i\xi) > \epsilon_{PTFE}(i\xi)$, enabling repulsive F_{C-L} for Au flakes, F_{C-L} is always attractive for an scheme effectively including Au, bromobenzene, and VO$_2$, as $\epsilon_{VO_2}(i\xi) > \epsilon_{bromobenzene}(i\xi)$. A similar scheme applies to the quantum trapping and release of a PTFE nanoplate under the reverse insulator-to-metal transition of VO$_2$. The proposed Casimir-Lifshitz force-based optical resonator can be tuned by external stimuli and offers promising capabilities for studying novel nano-scale physical and chemical phenomena. Furthermore, the design allows for the development of switchable devices for use in NEMS and MEMS.

3. Emergent Experimental Approaches

In recent years, there have been three innovative experiments based on the F_{C-L} in the plane-parallel geometry with fluids. **Table 1** provides a comparison of the details of each experimental system. All three experiments used a few micrometers wide and a few tens of nanometers thick Au flake that faced a highly reflective Au substrate. In all the experiments, an attractive F_{C-L} was present between the flake and the substrate. The main difference from one experiment to another was the approach used to compensate for this attractive force with a repulsive interaction. In all these systems, a sub-micrometric Fabry-Pérot cavity is formed between the flake and the substrate due to the balance of all forces acting on the suspended flake. Interestingly, each experiment proposed a way to fine-tune the size of such optical cavity either permanently, for a given sample, or dynamically. This self-assembled sub-micrometric resonator could potentially be utilized as a platform for exploring diverse fields such as nanophotonics, ultrasensitive sensing, and sub-micrometric tribology, among others.

In 2019, R. Zhao et al.[137] conducted a pioneering experiment based on the F_{C-L} in the plane-parallel geometry, involving a resonator made of two Au surfaces separated by a sub-micrometer gap properly stratified and filled with ethanol (Table 1 provides additional details). Similarly to our theoretical proposal scheme,[138] the dielectric function of the materials fulfil the condition $\epsilon_{Au}(i\xi) > \epsilon_{ethanol}(i\xi) > \epsilon_{Teflon}(i\xi)$. Thus, F_{C-L} between the Au flake and the PTFE -coated Au mirror in ethanol is repulsive at short separations and attractive at large ones. By using a spectrometer (**Figure 4a**) and measuring reflectance spectra of the assembled optical resonator in the optical regime (Figure 4b), the equilibrium distance at which the flake levitates over the substrate is obtained. As the intensity of the repulsive F_{C-L} increases with the thickness of the PTFE coating, the authors' strategy for tuning the flake trapping distance is to deposit different coating thicknesses (Figure 4c). This way, the penetration of the field is adjusted, and hence, the total force acting on the system, thereby fine-tuning the trapping distance. This modulation of the trapping distance is static, with each coating thickness corresponding to a highly stable trapping distance. The experiment by R. Zhao et al. represents a milestone in the field of Casimir science, exemplifying the first experimental demonstration of repulsive F_{C-L} in plane-parallel geometry, and is a benchmark that will inspire future experiments. This experiment opens the door to perform dispersion force measurements for any homogeneous material even if the optical constants of the materials are not known for a sufficiently large frequency range. Given its optical response in the narrow frequency range for spectrum fitting, the strength of the interaction, whether attractive or repulsive, can be measured indirectly by simply placing a layer of the test material under the coating of the Au substrate and re-measuring again the equilibrium distance.

In a second experiment in 2020 by B. Munkhbat et al.,[140] a repulsive F_{el} is used to balance the attractive F_{C-L} component
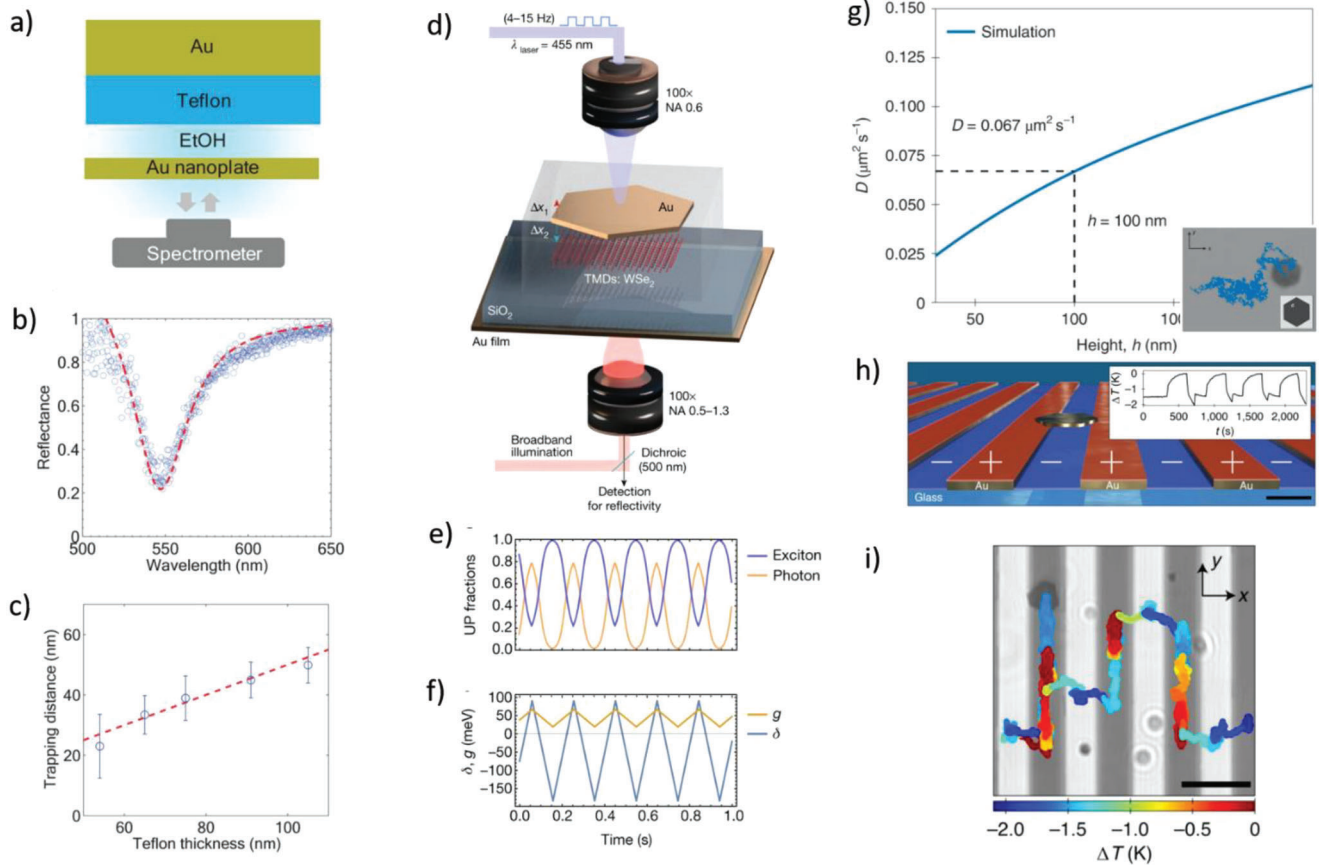
Figure 4. a) By measuring the reflectance from an area of 5 mm in diameter at the center of the Au nanoplate, the distance between the Au nanoplate and the PTFE surface can be determined by the Fabry-Pérot resonance in the reflectance spectrum. b) Reflectance spectrum for a sample with a PTFE thickness of 91 nm. c) Trapping distance versus PTFE thickness. The experimental results were averaged over multiple measurements of multiple trapped particles. Error bars show the variation of the average position of multiple trapped particles. Because the PTFE thickness is precisely measured using the ellipsometer and confirmed using AFM, none of the error bars show the PTFE thickness variation. The dashed line is the theoretical prediction. Adapted with permission.[137] Copyright 2019 Science. d) Schematic of the setup for active tuning of the microcavity by modulating the position of the floating gold flake along the vertical direction (that is, moving an extent Δx_1 and Δx_2 in the directions shown) with a control laser. e) Extracted excitonic and photonic fractions for the upper polariton, and f), its coupling strength (g, orange) and detuning (δ, grey-blue). Adapted with permission.[140] Copyright 2020 Nature Publishing Group. g) Theoretical diffusion D of a hexagonal flake with side a = 840 nm as a function of its height h above the surface obtained from hydrodynamic simulations. The experimentally measured D = 0.067 $\mu m^2 s^{-1}$ corresponds to height h = 100 nm. h) Hydrophobic gold stripes (thickness 30 nm, width 3 μm, separation 3 μm) nanofabricated on a hydrophilic glass substrate with a hydrophilic gold flake (a = 1450 nm) floating above. Inset: periodic raising and lowering of the temperature T to and away from the critical temperature Tc. The black scale bar corresponds to 2 μm. i) Full trajectory of the flake under periodic heating and cooling of the sample, showing that transitions occur shortly after reaching T ≈ Tc. Its starting point is marked by the particle image. Scale bars 6 μm. Adapted with permission.[141] Copyright 2022 Nature Publishing Group.

between the Au flakes that form the optical cavity. The F_{el} stems from the ion surface charges of the same sign of the interacting surfaces in water, leading to a double layer interaction between them. Flakes immersed in a water solution of ligand molecules (centrimonium bromide, CTAB) self-assembles in i) dimmers and trimers or ii) gets trapped over a SiO_2-coated Au substrate (refer to sketch (b) in Table 1). The ligands attached to the surfaces screen the surface charges. Therefore, the higher the ligand concentration, the less intense the repulsive electrostatic interaction that compensate the attractive F_{C-L} and, consequently, the smaller the cavity size. As in the experiment by R. Zhao et al.,[137] here the equilibrium distance between the two planar objects is determined indirectly through spectroscopic measurements. The SiO_2 coating is used solely to increase the size of the optical cavity between the flake and the Au substrate, which enhances

the Q-factor of the optical modes, improving the accuracy of the measurements. Regarding cavity tunability, B. Munkhbat et al. propose a faster way to dynamically change the cavity size based on the radiation pressure exerted by a laser impinging on the flake (Figure 4d), which can tune the cavity size within 0.1 seconds. As a proof-of-concept, the authors brilliantly demonstrate the utility of the self-assembled optical cavities by employing them as a platform to study the strong-coupling phenomenon. A 2D excitonic material that absorbs light in the visible range is deposited on the SiO_2-coated Au substrate. By displacing the flake with a laser, the size of the cavity is changed allowing the resonance of the cavity to be tuned to couple the absorption frequencies of the material inside the cavity. This coupling, named as light-matter strong coupling, results in the formation of hybrid energy states called polaritons.[168] Interestingly, the exciton

ADVANCED
SCIENCE NEWS

www.advancedsciencenews.com

ADVANCED
PHYSICS
RESEARCH
Open Access

www.advphysicsres.com

or photon composition of the upper polariton, and the strength of the coupling and detuning can be modulated by simply tuning the cavity size, allowing for control of the system in and out of the light-matter strong coupling regime (refer to Figure 4e,f). This has implications for photochemical rate reactions and opens up new pathways for these reactions enabled by polaritons.[181] These results pave the way for employing these passively assembled optical cavities as a platform to study in depth the strong coupling phenomenon and photochemical reactions in fluids, with an easy and fast way to control the coupling strength. Furthermore, the dimers and trimers formed by the flakes, whose spectral characteristics are particular, are considered as highly sensitive mobile and local sensors in those structures, capable of detecting variations in the concentration of ligands or ions in solution via the size of the optical cavity they form.

Finally, in a recent experiment in 2022, F. Schmidt et al.[141] exploit the repulsive critical Casimir force to trap a Au flake in an oily fluid consisting of a binary liquid mixture of water and lutidine, over a reflective substrate. The critical Casimir force,[40–42] which is the thermodynamic analog of the Casimir effect, leads to an effective force between two bodies immersed in a binary liquid mixture near a second-order phase transition. This force arises due to the confinement of the thermal fluctuations of the local concentration of one of the mixing components. The intensity of the critical Casimir force can be controlled by adjusting the temperature of the system around the critical temperature at which the binary liquid undergoes a second-order phase transition. In their experiment, the critical temperature is 34 °C. In addition, the critical Casimir force is repulsive if the surfaces of the bodies have opposite hydrophilic or hydrophobic characteristics, so the authors deposited self-assembled monolayers (SAMs) on the Au mirror to control surface adsorption. Therefore, the vertical positioning of the flake, which determines the size of the optical cavity between the flake and the reflecting substrate, is controlled through the chemical surface treatment and small variations of temperature. Those variations in temperature barely affect F_{C-L} when the system is ≈0.5 to 1 K below the critical temperature, whereas it implies significant variations in the Casimir-Lifshitz force as the critical temperature is approached. As a novelty, the authors developed a new method to determine the equilibrium distance based on the diffusive motion of the flake over the substrate (Figure 4g). Spectroscopic measurements were also used to validate the results. The new model proposed in this experiment provides an excellent platform for nanotribology studies of the flake-fluid-substrate system. It allows for quick determination of the distance between parallel surfaces (in a few seconds) and analysis of their movement when acted upon by other forces. The authors also demonstrate the potential for full control of micrometric objects by manipulating the lateral displacement of the flake via alternating hydrophilic and hydrophobic substrate surfaces (Figure 4h) and tuning the critical Casimir force in the vertical direction. In this context, the control of adhesion with temperature and the displacement and positioning of micrometric objects in all 3D by almost passive trapping of the object is becoming a reality (Figure 4i).

4. Outlook

The implementation of new optics-based approaches has enabled recent experiments in the plane-parallel geometry to measure separation distances between two objects under the action of F_{C-L} using far-field standard optical techniques. These experiments pave the way for observing quantum interactions in the nano- and micro-scale. Inspired by these systems, a wide variety of phenomena can be studied from an innovative experimental approach, promising gain of deeper insight into these phenomena and future applications in nanotechnology. By employing spectroscopic measurements or tracking the 2D diffusion of a micrometric object with an optical microscope, it is possible to control the movement of two interfaces toward or away from each other at the nano- and micro-scale and adjust the stiffness of the interaction. This can prove beneficial in accelerometers, gravimeters, or fundamental physics as nanotribology, but also in microfluidic NEMS and MEMS for sensing. Indeed, the employment of the repulsive F_{C-L} to avoid the friction between movable
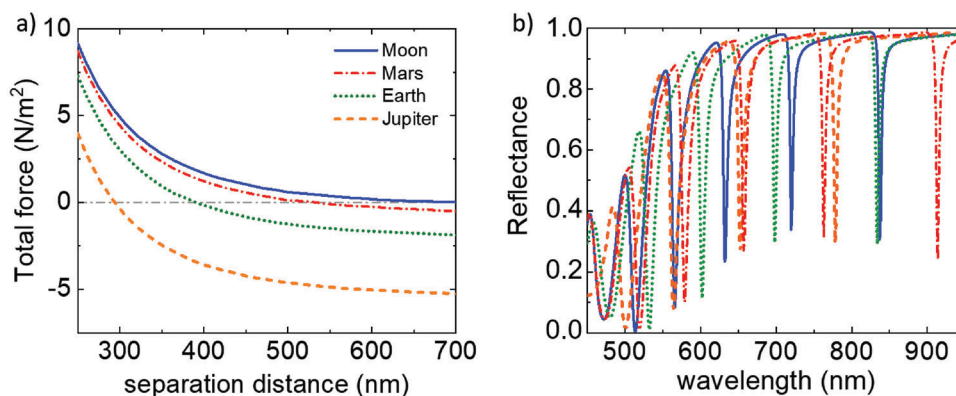

Figure 5. a) Total force between an Au-PS (30 nm – 1500 nm) bilayer immersed in glycerol over a gold substrate coated with 1000 nm of SiO$_2$, as a function of their separation distance. The dash dot horizontal line represents the total force equal zero. The gravity acceleration values at the surface of the solar objects are: Moon (1,62 m·s^{-2}), Mars (3,71 m·s^{-2}), The Earth (9,81 m·s^{-2}), and Jupiter (24,79 m·s^{-2}). The separation distances at which each curve intersect the zero total force correspond to the stable trapping distances and correspond to 294, 390, 527, and 682 nm, accordingly, for the different solar objects. b) The corresponding reflectance spectra (same color code as in Figure 4a) for the Casimir-Lifshitz optical resonators operating in quantum trapping mode.

**ADVANCED
SCIENCE NEWS**

www.advancedsciencenews.com

**ADVANCED
PHYSICS
RESEARCH**

www.advphysicsres.com

parts of NEMS and MEMS have been extensively studied in the literature, with the ultimate goal of creating ultrasensitive nanomachines and sensors. Experimentally, this approach is limited by the use of a fluid material mediating the interaction between two bodies. However, finding realistic and man-made materials that give rise a repulsive F_{C-L} when separated by vacuum or air would revolutionize the performance of NEMS and MEMS, which currently suffer from jump-to-contact instability and friction effects resulting from the attractive nature of the force.

Just as an example of the technological potential of self-assembled Casimir-Lifshitz optical cavities, micrometric portable gravimeters capable of detecting variations in gravity values throughout the Solar System could be devised. A cavity with a structure similar to the one considered,[138] consisting of a PS-Au bilayer suspended in glycerol over a SiO_2 coated Au substrate, might display trapping distances ranging from nano- to micro-meters, as shown in **Figure** 5a, as a result of the variation of the gravity force values at the surface of the different planets. Changes in the equilibrium position of the levitating upper mirror will translate into significant modifications of the reflectance spectra of the Casimir-Lifshitz optical resonators, as shown in Figure 5b, providing a precise measurement of *g*. In this regard, the accuracy of the proposed system is higher for smaller values of gravitational acceleration. Thus, for g values between the ones for the Moon or Mars, the equilibrium distance changes ≈70 nm per gravitational acceleration unit, whereas the variation of the equilibrium distance is only ≈6 nm per gravitational acceleration unit when considering g values between the ones for the Earth and Jupiter. The precision attainable in measuring gravitational acceleration depends not only on the steepness of the force curve concerning the separation distance, but also on the Q-factor of the optical modes sustained by the formed optical resonator. Notably, among the considered celestial bodies, the highest level of precision for gravitational acceleration measurements will be achieved when measuring gravity on Moon.

5. Conclusions

After decades of research attempting to experimentally demonstrate and accurately measure F_{C-L}, recent experiments have achieved success by forming tunable optical resonators in fluids using the quantum trapping of a metallic flake through the balance of an attractive F_{C-L} component and other forces. This approach, which can be applied to planar architectures (retrieving its potential for the highest intensity forces), offers a range of possibilities in various fields, including self-assembly, non-contact machinery, and high-precision sensors. Tunable optical resonators are a versatile platform for studying fundamental phenomena and developing micro- and nano-technological applications. In addition to measuring F_{C-L} for any synthesizable thin material, these resonators can be used to investigate strong light-matter coupling in fluids, tribological properties of coatings and planar objects, and more. The far-field interrogating techniques used in these experiments can be extended to NEMS and MEMS, such as micro-gravimeters or nanomachinery, whereas low invasive deterministic positioning of nano- and microsensors can be also envisaged.

Conflict of Interest

The authors declare no conflict of interest.

Data Availability Statement

The data that support the findings of this study are available from the corresponding author upon reasonable request.

[1] H. B. G. Casimir, *Proc. K. Ned. Akad. Wet.* **1948**, *60*, 793.
[2] V. A. Parsegian, *Van der Waals Forces: a Handbook for Biologists, Chemists, Engineers, and Physicists*, Cambridge University Press, **2005**.
[3] H. B. G. Casimir, D. Polder, *Phys. Rev.* **1948**, *73*, 360.
[4] E. M. Lifshitz, *Sov. Phys. JETP* **1956**, *2*, 73.
[5] I. E. Dzyaloshinskii, E. M. Lifshitz, L. P. Pitaevskii, *Adv. Phys.* **1961**, *10*, 165.
[6] K. Milton, *Int. J. Mod. Phys. A* **2022**, *37*, 2202001.
[7] G. Bimonte, T. Emig, N. Graham, M. Kardar, *Annu. Rev. Nucl. Part. Sci.* **2022**, *72*, 93.
[8] G. L. Klimchitskaya, U. Mohideen, V. M. Mostepanenko, *Rev. Mod. Phys.* **2009**, *81*, 1827.
[9] L. M. Woods, D. A. R. Dalvit, A. Tkatchenko, P. Rodriguez-Lopez, A. W. Rodriguez, R. Podgornik, *Rev. Mod. Phys.* **2016**, *88*, 045003.
[10] L M. Woods, M. Krüger, V V. Dodonov, *Appl. Sci.* **2021**, *11* 293.
[11] J. Fiedler, K. Berland, J. W. Borchert, R. W. Corkery, A. Eisfeld, D. Gelbwaser-Klimovsky, M. M. Greve, B. Holst, K. Jacobs, M. Krüger, D. F. Parsons, C. Persson, M. Presselt, T. Reisinger, S. Scheel, F. Stienkemeier, M. Tømterud, M. Walter, R. T. Weitz, J. ZaliVeckas, *Phys. Chem. Chem. Phys.* **2023**, *25*, 2671.
[12] T. Gong, M R. Corrado, A R. Mahbub, C. Shelden, J N. Munday, *Nanophotonics* **2021**, *10*, 523.
[13] A. Stange, D K. Campbell, D J. Bishop, *Phys. Today* **2021**, *74*, 42.
[14] C. M. Wilson, G. Johansson, A. Pourkabirian, M. Simoen, J. R. Johansson, T. Duty, F. Nori, P. Delsing, *Nature* **2011**, *479*, 376.
[15] F. C. Lombardo, F. D. Mazzitelli, A. Soba, P. I. Villar, *Phys. Rev. A* **2018**, *98*, 022512.
[16] V. Dodonov, *Physics* **2020**, *2* 67.
[17] F. Intravaia, M. Oelschläger, D. Reiche, D. A. R. Dalvit, K. Busch, *Phys. Rev. Lett.* **2019**, *123*, 120401.
[18] D. Reiche, F. Intravaia, J.-T. Hsiang, K. Busch, B. L. Hu, *Phys. Rev. A* **2020**, *102*, 050203(R).

**ADVANCED
SCIENCE NEWS**

www.advancedsciencenews.com

**ADVANCED
PHYSICS
RESEARCH**

www.advphysicsres.com

[19] M. B Farías, F C. Lombardo, A. Soba, P I. Villar, R S. Decca, *npj Quantum Inf.* **2020**, *6*, 25.

[20] F C. Lombardo, R S. Decca, L. Viotti, P I. Villar, *Adv. Quantum Technol.* **2021**, *4*, 2000155.

[21] X. Guo, K. A. Milton, G. Kennedy, W. P. McNulty, N. Pourtolami, Y. Li, *Phys. Rev. D* **2021**, *104*, 116006.

[22] M. Oelschläger, D. Reiche, C. H. Egerland, K. Busch, F. Intravaia, *Phys. Rev. A* **2022**, *106*, 052205.

[23] D. Reiche, F. Intravaia, K. Busch, *APL Photonics* **2022**, *7*, 030902.

[24] K. Autumn, M. Sitti, Y A. Liang, A M. Peattie, W R. Hansen, S. Sponberg, T W. Kenny, R. Fearing, J N. Israelachvili, R J. Full, *Proc. Natl. Acad. Sci. U. S. A.* **2002**, *99*, 12252.

[25] K. Autumn, *Am. Sci.* **2006**, *94*, 124.

[26] Israelachvili, J. N., *Intermolecular and surface forces*, Academic Press, **2011**.

[27] M. Elbaum, M. Schick, *Phys. Rev. Lett.* **1991**, *66*, 1713.

[28] M. Baker, J. Dash, *J. Cryst. Grow.* **1989**, *97*, 770.

[29] J. G. Dash, J. S. Wettlaufer, *Can. J. Phys.* **2003**, *81*, 201.

[30] S C. Sherwood, V T. J. Phillips, J. S. Wettlaufer, *Geophys. Res. Lett.* **2006**, *33*, L05804.

[31] J. S. Wettlaufer, *Philos. Trans. R. Soc., A* **2019**, *377*, 20180261.

[32] L. A. Wilen, J. G. Dash, *Phys. Rev. Lett.* **1995**, *74*, 5076.

[33] J. G. Dash, H. Fu, J. S. Wettlaufer, *Rep. Prog. Phys.* **1995**, *58*, 115.

[34] J. G. Dash, A. W. Rempel, J. S. Wettlaufer, *Rev. Mod. Phys.* **2006**, *78*, 695.

[35] D T.F Möhlmann, *Icarus* **2004**, *168*, 318.

[36] D T.F. Möhlmann, *Icarus* **2008**, *195*, 131.

[37] H. Hansen-Goos, E. S. Thomson, J. Wettlaufer, *Planet. Space Sci.* **2014**, *98*, 169.

[38] M. Boström, V. Esteso, J. Fiedler, I. Brevik, S. Y. Buhmann, C. Persson, S. Carretero-Palacios, D F. Parsons, R W. Corkery, *Astron. Astrophys.* **2021**, *650*, A54.

[39] S K. Lamoreaux, *Phys. Today* **2007**, *60*, 40.

[40] M. E. Fisher, P. G. Gennes, *C R Acad Sci III* **1978**, *287*, 207.

[41] A. Gambassi, *Journal of Physics: Conference Series IOP Publishing* **2009**, *161*, 012037.

[42] C. Hertlein, L. Helden, A. Gambassi, S. Dietrich, C. Bechinger *Nature*, **2008** *451*, 172.

[43] B B. Machta, S L. Veatch, J P. Sethna, *Phys. Rev. Lett.* **2012**, *109*, 138101.

[44] Y. Srivastava, A. Widom, M. H. Friedman. *Phys. Rev. Lett.* **1985**, *55* 2246.

[45] F. M. Serry, D. Walliser, G. J. Maclay, *J. Microelectromech. Syst.* **1995**, *4*, 193.

[46] F. M Serry, D. Walliser, G. J Maclay. *J. Appl. Phys.* **1998**, *84* 2501.

[47] H. B. Chan, V. A. Aksyuk, R. N. Kleiman, D. J. Bishop, F. Capasso, *Science* **2001**, *291*, 1941.

[48] J.-G. Guo, Y.-P. Zhao. *J. Microelectromech. Sys.* **2004**, *13*, 1027.

[49] W. H. Lin, Y. P. Zhao. *Chaos, Solitons Fractals* **2005**, *23* 1777.

[50] F. Pinto, *In AIP Conference Proceedings*, Vol. *969*, American Institute of Physics, **2008**, pp. 959–968.

[51] G. Palasantzas, M. Sedighi, V B. Svetovoy. *App. Phys. Lett.* **2020**, *117* 120501.

[52] J. Javor, Z. Yao, M. Imboden, D K. Campbell, D J. Bishop, *Microsyst. Nanoeng.* **2021**, *7*, 73.

[53] K. Nakata, K. Suzuki, *Phys. Rev. Lett.* **2023**, *130*, 096702.

[54] G. Palasantzas, V B. Svetovoy, *Int. J. Mod. Phys. A* **2022**, *37*, 2241001.

[55] C. Genet, A. Lambrecht, P. Maia Neto, S. Reynaud, *EPL* **2003**, *62*, 484.

[56] W. Broer, G. Palasantzas, J. Knoester, V B. Svetovoy, *Phys. Rev. B* **2012**, *85*, 155410.

[57] I A. Soldatenkov, A A. Yakovenko, V B. Svetovoy, *Universe* **2021**, *7*, 64.

[58] R. S. Decca, D. López, E. Fischbach, G. L. Klimchitskaya, D. E. Krause, V. M. Mostepanenko. *Ann. Phys.* **2005**, *318* 37.

[59] R. O. Behunin, F. Intravaia, D. A. R. Dalvit, P. A. M Neto, S. Reynaud, S. Reynaud, *Phys. Rev. A* **2012**, *85*, 012504.

[60] R. O. Behunin, D. A. R. Dalvit, R. S. Decca, C. Genet, I. W. Jung, A. Lambrecht, A. Liscio, D. López, S. Reynaud, G. Schnoering, G. Voisin, Y. Zeng, *Phys. Rev. A* **2014**, *90*, 062115.

[61] J. L. Garrett, D. Somers, J. N. Munday, *J. Phys.: Condens. Matter* **2015**, *27*, 214012.

[62] J L. Garrett, J. Kim, J N. Munday, *Phys. Rev. Res.* **2020**, *2*, 023355.

[63] J. N. Munday, F. Capasso, V. A. Parsegian, S. M. Bezrukov, *Phys. Rev. A* **2008**, *78*, 032109.

[64] V. A Parsegian, D. Gingell. *Biophys. J.* **1972**, *12* 1192.

[65] B. Cappella, G. Dietler. *Surf. Sci. Rep.* **1999**, *34*, 1.

[66] S. K. Lamoreaux, *Phys. Rev. Lett.* **1997**, *78*, 5.

[67] U. Mohideen, A. Roy, *Phys. Rev. Lett.* **1998**, *81*, 4549.

[68] G. L. Klimchitskaya, A. Roy, U. Mohideen, V. M. Mostepanenko, *Phys. Rev. A* **1999**, *60*, 3487.

[69] A. Roy, C.-Y. Lin, U. Mohideen, *Phys. Rev. D* **1999**, *60*, 111101R.

[70] B. W. Harris, F. Chen, U. Mohideen, *Phys. Rev. A* **2000**, *62*, 052109.

[71] F. Chen, G. L. Klimchitskaya, U. Mohideen, V. M. Mostepanenko *Phys. Rev. A* **2004**, *69*, 022117.

[72] H. B. Chan, V. A. Aksyuk, R. N. Kleiman, D. J. Bishop, F. Capasso, *Science* **2001**, *291*, 1941.

[73] H. B. Chan, V. A. Aksyuk, R. N. Kleiman, D. J. Bishop, F. Capasso, *Phys. Rev. Lett.* **2001**, *87*, 211801.

[74] R. S. Decca, E. Fischbach, G. L. Klimchitskaya, D. E. Krause, D. López, V. M. Mostepanenko, *Phys. Rev. D* **2003**, *68*, 116003.

[75] R. S. Decca, D. López, E. Fischbach, D. E. Krause, *Phys. Rev. Lett.* **2003**, *91*, 050402.

[76] R. S. Decca, D. López, H. B. Chan, E. Fischbach, G. L. Klimchitskaya, D. E. Krause, V. M. Mostepanenko, *J. Low Temp. Phys.* **2004**, *135*, 63.

[77] R. S. Decca, D. López, H. B. Chan, E. Fischbach, D. E. Krause, C. R. Jamell, *Phys. Rev. Lett.* **2005**, *94*, 240401.

[78] R. S. Decca, D. López, E. Fischbach, G. L. Klimchitskaya, D. E. Krause, V. M. Mostepanenko, *Phys. Rev. D* **2007**, *75*, 077101.

[79] R. S. Decca, D. López, E. Fischbach, G. L. Klimchitskaya, D. E. Krause, V. M. Mostepanenko, *Eur. Phys. J. C* **2007**, *51*, 963

[80] A. Milling, P. Mulvaney, I. Larson. *J. Colloid Interface Sci.* **1996**, *180*, 460.

[81] A. Meurk, P F. Luckham, L. Bergström, L. Bergstrom. *Langmuir*, **1997**, *13*, 3896.

[82] J. N. Munday, F. Capasso, V. A Parsegian, *Nature* **2009**, *457*, 170.

[83] G. L. Klimchitskaya, V. M. Mostepanenko, *Mod. Phys. Lett. A* **2020**, *35*, 2040007.

[84] M. Liu, Y. Zhang, G. L. Klimchitskaya, V. M. Mostepanenko, U. Mohideen, *Phys. Rev. B* **2021**, *104*, 085436.

[85] G. Bimonte, B. Spreng, P A. Maia Neto, G.-L. Ingold, G L. Klimchitskaya, V M. Mostepanenko, R S. Decca, *Universe* **2021**, *7*, 93.

[86] F. Chen, U. Mohideen, G. L. Klimchitskaya, V. M. Mostepanenko, *Phys. Rev. A* **2005**, *72*, 020101R.

[87] F. Chen, G. L. Klimchitskaya, V. M. Mostepanenko, U. Mohideen, *Opt. Express* **2007**, *15*, 4823.

[88] F. Chen, G. L. Klimchitskaya, V. M. Mostepanenko, U. Mohideen, *Phys. Rev. Lett.* **2006**, *97*, 170402.

[89] F. Chen, U. Mohideen, G. L. Klimchitskaya, V. M. Mostepanenko, *Phys. Rev. A* **2006**, *74*, 022103.

[90] F. Chen, G. L. Klimchitskaya, V. M. Mostepanenko, U. Mohideen, *Phys. Rev. B* **2007**, *76*, 035338.

[91] J. M. Obrecht, R. J. Wild, M. Antezza, L. P. Pitaevskii, S. Stringari, E. A. Cornell, *Phys. Rev. Lett.* **2007**, *98*, 063201.

[92] A. O. Sushkov, W. J. Kim, D. A. R. Dalvit, S. K. Lamoreaux, *Nat. Phys.* **2011**, *7*, 230.

[93] F. Intravaia, S. Koev, I. W. Jung, A. Talin, P. Davids, R. Decca, V. Aksyuk, D. A. R. Dalvit, D. Lopez, *Nat. Commun.* **2013**, *4*, 09.

[94] A. Noto, R. Messina, B. Guizal, M. Antezza. *Phys. Rev. A* **2014**, *90* 022120.

[95] M. Wang, L. Tang, C. Y. Ng, R. Messina, B. Guizal, J. A. Crosse, M. Antezza, C. T. Chan, H. B. Chan, *Nat. Commun.* **2021**, *12*, 600.

[96] G. Torricelli, P. J. van Zwol, O. Shpak, C. Binns, G. Palasantzas, B. J. Kooi, V. B. Svetovoy, M. Wuttig, *Phys. Rev. A* **2010**, *82*, 010101.

[97] G. Torricelli, P J. Van Zwol, O. Shpak, G. Palasantzas, V B. Svetovoy, C. Binns, B J. Kooi, P. Jost, M. Wuttig, *Adv. Funct. Mater.* **2012**, *22* 3729.

[98] A D. Phan, N. A. Viet, N A. Poklonski, L M. Woods, C H. Le, *Phys. Rev. B* **2012**, *86*, 155419.

[99] M. Sedighi, W. H. Broer, G. Palasantzas, B. J. Kooi, *Phys. Rev. B* **2013**, *88*, 165423.

[100] C. Abbas, B. Guizal, M. Antezza, *Phys. Rev. Lett.* **2017**, *118*, 126101.

[101] N. Khusnutdinov, R. Kashapov, L. M. Woods, *2D Mater.* **2018**, *5*, 035032.

[102] F. Chen, G. L. Klimchitskaya, V. M. Mostepanenko, U. Mohideen, U. Mohideen, *Phys. Rev. B* **2007**, *76* 035338.

[103] J. Wang, X. Zhang, S.-Y. Pei, Da-He Liu. *Phys. Rev. A* **2006**, *73* 042103.

[104] Ge Song, Z. Liu, L. Jia, C. Li, Y. Chang, *Nanomaterials* **2022**, *12* 2168.

[105] T.-B. Wang, Y. Zhou, H.-Q. Mu, K. Shehzad, De-J Zhang, W.-X. Liu, T.-B. Yu, Q.-H. Liao, *Nanotechnology* **2022**, *33*, 245001.

[106] R. Zhao, J. Zhou, Th. Koschny, E. N. Economou, C. M. Soukoulis. *Phys. Rev. Lett.* **2009**, *103*, 103602.

[107] T. Oosthuys, D. Dudal, arXiv:2301.12870v3.

[108] F. S. S. Rosa, D. A. R. Dalvit, P. W. Milonni. *Phys. Rev. A* **2008**, *78* 032117.

[109] C. Shelden, B. Spreng, J. N. Munday, arXiv:2302.00865v1.

[110] N. Khusnutdinov, L. M. Woods, *JETP Lett.* **2019**, *110*, 183.

[111] L. Wang, H. Sun, Y. Jia, L. Ge, Z. Ji, Ke Gong, *Opt. Express* **2023**, *31*, 15204.

[112] D. Drosdoff, L M. Woods *Phys. Rev. B* **2010**, *82*, 155459.

[113] P. Rodriguez-Lopez, W J. M. Kort-Kamp, D A. R. Dalvit, L M. Woods. *Nat. Commun.* **2017**, *8*, 14699.

[114] C. H. Egerland, K. Busch, F. Intravaia, *Phys. Rev. B* **2019**, *100*, 235418.

[115] G. L. Klimchitskaya, U. Mohideen, V. M. Mostepanenko, *Int. J. Mod. Phys. A* **2022**, *37*, 2241003.

[116] F. Zhou, L. Spruch, *Phys. Rev. A* **1995**, *52*, 297.

[117] R. Esquivel-Sirvent, C. Villarreal, G. H. Cocoletzi, *Phys. Rev. A* **2001**, *64* 052108.

[118] R. Esquivel-Sirvent, C. Villarreal, W. L. Mochán, G. H. Cocoletzi. *Phys. Status Solidi (b)* **2022**, *230*, 409.

[119] C. Raabe, L. Knoll, D. G. Welsch, *Phys. Rev. A* **2002**, *68*, 12.

[120] V. Esteso, S. Carretero-Palacios, H. Míguez, *Phys. Rev. A* **2020**, *101*, 033815.

[121] R. Esquivel-Sirvent, G C. Schatz, *Phys. Rev. A* **2011**, *83* 042512.

[122] Y. Ye, Q. Hu, Q. Zhao, Y. Meng, *Phys. Rev. B* **2018**, *98* 035410.

[123] V. Esteso, S. Carretero-Palacios, H. Míguez, *J. Phys. Chem. Lett.* **2022**, *13*, 4513.

[124] A V. Postnikov, I V. Uvarov, V B. Svetovoy, *Rev. Sci. Instrum.* **2023**, *94*, 043907.

[125] Z. Xu, P. Ju, X. Gao, K. Shen, Z. Jacob, T. Li, *Nat. Commun.* **2022**, *13*, 6148.

[126] D. S. Ether Jr., L. B. Pires, S. Umrath, D. Martinez, Y. Ayala, B. Pontes, G. R. de S. Araujo, S. Frases, G.-L. Ingold, F. S. S. Rosa, N. B. Viana, H. M. Nussenzveig, P. A. M Neto, *EPL* **2015**, *112*, 44001.

[127] L. B. Pires, D. S. Ether, B. Spreng, G. R. S. Araújo, R. S. Decca, R. S. Dutra, M. Borges, F. S. S. Rosa, G.-L. Ingold, M. J. B. Moura, S. Frases, B. Pontes, H. M. Nussenzveig, S. Reynaud, N. B. Viana, P. A. M Neto, *Phys. Rev. Res.* **2021**, *3*, 033037.

[128] A. Kundu, S. Paul, S. Banerjee, A. Banerjee, *Appl. Phys. Lett.* **2019**, *115*, 123701.

[129] A W. Rodriguez, J. N. Munday, J. D. Joannopoulos, F. Capasso, D A. R. Dalvit, S G. Johnson, *Phys. Rev. Lett.* **2008**, *101* 190404.

[130] A W. Rodriguez, D. Woolf, A P. Mccauley, F. Capasso, J D. Joannopoulos, S G. Johnson, *Phys. Rev. Lett.* **2010**. *105* 060401.

[131] A W. Rodriguez, A P. Mccauley, D. Woolf, F. Capasso, J. D. Joannopoulos, S G. Johnson, *Phys. Rev. Lett.* **2010**, *104*, 160402.

[132] N. Inui, *J. Appl. Phys.* **2012**, *111*, 074304.

[133] M. Dou, F. Lou, M. Boström, I. Brevik, C. Persson. *Phys. Rev. B* **2014**, *89*, 201407(R).

[134] A. W. Rodriguez, P. C. Hui, D. P. Woolf, S. G. Johnson, M. Lončar, F. Capasso, *Ann. Phys.* **2015**, *527* 45.

[135] V. Esteso, S. Carretero-Palacios, H. Míguez, *J. Phys. Chem. C* **2015**, *119*, 5663.

[136] V. Esteso, S. Carretero-Palacios, P. Thiyam, H. Míguez, D. F. Parsons, I. Brevik, M. Boström, *Langmuir* **2019**, *35* 4218.

[137] R. Zhao, L. Li, S. Yang, W. Bao, Y. Xia, P. Ashby, Y. Wang, X. Zhang, *Science* **2019**, *7*, 984.

[138] V. Esteso, S. Carretero-Palacios, H. Míguez, *J. Phys. Chem. Lett.* **2019**, *10*, 5856.

[139] L. Ge, Xi Shi, Z. Xu, Ke Gong, *Phys. Rev. B* **2020**, *101*, 104107.

[140] B. Munkhbat, A. Canales, B. Küçüköz, D G. Baranov, T O. Shegai. *Nature* **2021**, *597*, 214.

[141] F. Schmidt, A. Callegari, A. Daddi-Moussa-Ider, B. Munkhbat, R. Verre, T. Shegai, M. Käll, H. Löwen, A. Gambassi, G. Volpe, *Nat. Phys.* **2023**, *19*, 271.

[142] J. Feist, *Nature* **2021**, *597*, 185.

[143] V. Esteso Carrizo, *Nat. Phys.* **2023**, *19*, 161.

[144] A W. Rodriguez, D. Woolf, P.-C. Hui, E. Iwase, A P. Mccauley, F. Capasso, M. Loncar, S G. Johnson, *App. Phys. Lett.* **2011**, *98*, 194105.

[145] P. W. Milonni, *The quantum vacuum: an introduction to quantum electrodynamics*, Elsevier Science, San Diego **2013**.

[146] K. Schram. *Phys. Lett. A* **1973**, *43*, 282.

[147] M. Bordag, U. Mohideen, V. M. Mostepanenko. *Phys. Rep.* **2001**, *353*, 1.

[148] C. Genet, A. Lambrecht, S. Reynaud. *Phys. Rev. A* **2003**, *67*, 043811.

[149] M. S. Tomas. *Phys. Rev. A* **1995**, *51*, 2545.

[150] Bo E. Sernelius. *Phys. Rev. B* **2014**, *90*, 155457.

[151] P. R Buenzli, Ph. A Martin, *EPL* **2005**, *72*, 42.

[152] B. Jancovici, L. Šamaj *EPL* **2005**, *72*, 35.

[153] A W. Rodriguez, F. Capasso, S G. Johnson, *Nat. Photonics* **2011**, *5*, 211.

[154] A. Gusso, A. G. M. Schmidt, *Braz. J. Phys.* **2006**, *36*, 168.

[155] P S. Venkataram, S. Molesky, P. Chao, A W. Rodriguez, *Phys. Rev. A* **2020**, *101*, 052115.

[156] M. Boström, C. Persson, Bo E. Sernelius, *Eur. Phys. J. B* **2013**, *86*, 43.

[157] S. K. Lamoreaux, *Phys. Rev. A* **1999**, *59*, R3149(R).

[158] G. L. Klimchitskaya, U. Mohideen, V. M. Mostepanenko, *J. Phys. A: Math. Theor.* **2007**, *40*, F339.

[159] M. Soltanrezaee, M. Bodaghi, A. Farrokhabadi, *Sci. Rep.* **2019**, *9*, 11706.

[160] M. Camacho, T. Gong, B. Spreng, I. Liberal, N. Engheta, J N. Munday, *Phys. Rev. A* **2022**, *105*, L061501.

[161] A. E. Rubio López, V. Giannini, arXiv:2210.12094v1.

[162] S. Chu, J. E. Bjorkholm, A. Ashkin, J. P. Gordon, L. W. Hollberg, *Opt. Lett.* **1986**, *11*, 73.

[163] O M. Maragò, P H. Jones, P G. Gucciardi, G. Volpe, A C. Ferrari, *Nat. Nanotechnol.* **2013**, *8*, 807.

[164] A. S. Urban, S. Carretero-Palacios, A. A. Lutich, T. Lohmüller, J. Feldmann, F. Jäckel, *Nanoscale* **2014**, *6*, 4458.

[165] C J. Bustamante, Y R. Chemla, S. Liu, M D. Wang, *Nat. Rev. Methods Primers* **2021**, *1*, 25.

[166] G. Volpe, et al. arXiv:2206.13789v1.

[167] R. Esquivel-Sirvent, G C. Schatz, *J. Chem. Phys.* **2013**, *117*, 5492.

**ADVANCED
SCIENCE NEWS**

www.advancedsciencenews.com

**ADVANCED
PHYSICS
RESEARCH**
Open Access

www.advphysicsres.com

[168] D A. T. Somers, J L. Garrett, K J. Palm, J N. Munday, *Nature* **2018**, *564*, 386.

[169] P. Thiyam, P. Parashar, K. V. Shajesh, O. I. Malyi, M. Boström, K. A. Milton, I. Brevik, C. Persson, *Phys. Rev. Lett.* **2018**, *120*, 131601.

[170] F J. Garcia-Vidal, C. Ciuti, T W. Ebbesen, *Science* **2021**, *373*, 6551.

[171] D. P. Sheehan, *J. Chem. Phys.* **2009**, *131* 104706.

[172] A D. Dunkelberger, B S. Simpkins, I. Vurgaftman, J C. Owrutsky, *Annu. Rev. Phys. Chem.* **2022**, *73*, 429.

[173] R F. Ribeiro, L A. Martínez-Martínez, M. Du, J. Campos-Gonzalez-Angulo, J. Yuen-Zhou, *Chem. Sci.* **2018**, *9* 6325.

[174] J. Galego, F J. Garcia-Vidal, J. Feist, *Nat. Commun.* **2016**, *7*, 13841.

[175] J. Fregoni, S. Corni, M. Persico, G. Granucci, *J. Comput. Chem.* **2020**, *41*, 2033.

[176] P M. Dove, C M. Craven, *Geochim. Cosmochim. Acta* **2005**, *69*, 4963.

[177] M. Dasuya, T. Sogawa, T. Masuda, T. Kamijo, K. Uosaki, K. Kurihara, *J. Phys. Chem. C* **2016**, *120*, 15986.

[178] J. Stefan, *Sitzber. Akad. Wiss. Wien, Math. Naturw. Kl. Abt. II* **1874**, *69*, 713.

[179] J. J. Bikerman, *The Science of Adhesive Joints*, Academic Press, New York **1968**.

[180] B. He, Z. Wang, M. Li, K. Wang, R. Shen, S. Hu, *IEEE ASME Trans. Mechatron.* **2013**, *19*, 312.

[181] J A. Hutchison, T. Schwartz, C. Genet, E. Devaux, T W. Ebbesen, *Angew. Chem., Int. Ed.* **2012**, *51*, 1592.